Journal of Science and Transport Technology
Journal homepage: https://jstt.vn/index.php/en

Real-time Vehicle Behavior Classification using Single 3-Axis Magnetic Field Sensor and Neural Network

Vu Van Quang[1], Nguyen Van Tuan[1], Bui Hai Dang[1,2], Vu Toan Thang[1]*
[1]Precision Engineering & Smart Measurement Lab, School of Mechanical Engineering, Hanoi University of Science and Technology, No 1 Dai Co Viet Street, Hanoi 100000, Vietnam
[2]Faculty of Information Technology, University of Transport Technology, No 54 Trieu Khuc Street, Hanoi 100000, Vietnam

Article info
Type of article:
Original research paper

DOI:
https://doi.org/10.58845/jstt.utt.2025.en.5.3.98-111

***Corresponding author:**
Email address:
thang.vutoan@hust.edu.vn

Received: 17/03/2025
Received in Revised Form: 12/08/2025
Accepted: 05/09/2025

Abstract: This paper presents a real-time method for classifying vehicle behaviors, particularly related to lane violation behaviors by analyzing the output of magnetic sensors. The system assumes the sensor is installed beneath lane markings to detect magnetic field disturbances as vehicles approach. The feature extraction process emphasizes the vertical (Z-axis) magnetic field component and its declination angle, both of which demonstrate robust discriminative characteristics across different vehicle types and positions. A lightweight neural network classification model, based on those features, is trained on these features and deployed on embedded hardware to ensure rapid response and minimal power consumption. The proposed model achieves an overall accuracy of 89.75%, in distinguishing between legal (in-lane) and illegal (lane-crossing) vehicle behaviors. This work introduces a novel integration of simplified signal processing and efficient machine learning suitable for real-time deployment in low-cost Intelligent Transportation Systems (ITS), especially in dense or infrastructure-limited environments.

Keywords: Vehicle behavior, Magnetic field sensor, Magnetic vector declination, Neural network, Signal threshold detection.

1. Introduction

Intelligent Transportation Systems (ITS) play a crucial role roll in enhancing the efficacy, safety, and consistency of transportation infrastructure, effectively helping to reduce serious problems such as traffic jams and accidents. Most ITS solutions operate by gathering information. through various sensors, such as Lidar Tracking System, Induction loop detectors [1], Camera, Infrared System [2], etc., to monitor and analyze traffic characteristics such as vehicle flow [3], speed or even traffic violations. The advantages and disadvantages of those mentioned sensor systems have been discussed in numerous studies [4, 5].

Magnetic field sensors have also been widely adopted in ITS for tasks, such as vehicle detection and vehicle speed estimation [6]. Owing to their advantages of low cost, low power consumption, and compact size, magnetic field sensors present a viable alternative solution to overcome the drawbacks of other traditional systems [7]. ITS applications utilizing magnetic field sensors can be easily installed and scaled within the transportation infrastructure network. Several studies have

examined their applications, for instance, in [8], anisotropic magneto-resistive (AMR) sensors were placed on the road for vehicle identification and classification. In subsequent work, Vytautas Markevicius et al. proposed methods for estimating vehicle length by combining signal threshold detection with cross-correlation techniques for sensor signals in a dynamic environment. In another work, magnetic field sensors can even be installed on the roadside, aiming to estimate vehicle speed. It has been observed that, in aforementioned works, the full magnetic profile of the vehicle (from entry to exit over the sensor) is used for analysis. However, such approaches are unsuitable for applications that require real-time responses—such as immediate detection of lane violations. To address this limitation, this research proposes a new method using a magnetic field sensor system specifically designed to identify vehicle behaviors related to lane violation events.

This research direction is motivated by the frequent occurrence of lane violation behavior in Vietnam and similar contexts [9]. According to reports [10], lane violations are a significant contributor to severe traffic accidents in the country. The leading causes of these accidents include reckless driving and speeding. While improving traffic awareness among drivers is important, it is equally necessary to detect and penalize violations effectively—especially on highways and in dense urban areas.

In the proposed system, embedded devices equipped with 3-axis magnetic sensors are installed beneath the road surface and positioned directly between lane markings. This design ensures minimal disruption to traffic while maintaining sensitivity to vehicle movement across or along the lane boundary. The system operates independently, with wireless communication between modules to allow scalability, compactness, and ease of deployment.

The main contribution of this work lies in proposing a novel integration of lightweight signal processing and machine learning techniques for real-time lane violation detection. Rather than analyzing the entire magnetic signal profile, our approach extracts feature from only the initial part of the magnetic signal—enabling instant classification. We focus on the vertical magnetic field component (Z-axis) and its angular variation (declination) due to their strong discriminative properties. Although there are many neural networks used such as FNN (Feedforward Neural Network) [11] or a type of FNN is MLP (Multi-layer Perceptron) [12], or CNN (Convolutional Neural Network) [13,14]. A lightweight neural network specifically MLP because the data obtained from the magnetic field sensor is only digital data sent back periodically, consisting of a single hidden layer with six neurons, is employed to classify two behaviors: (LEGAL – LEG) vehicles passing within the correct lane, and (ILLEGAL – ILL) vehicles crossing the lane boundary. This neural model is optimized for real-time processing on low-power embedded platforms and achieves classification latency under 20 milliseconds.

A primary technical challenge lies in distinguishing cases where small vehicles pass directly overhead from cases where larger vehicles pass nearby, as their magnetic signatures can be deceptively similar. Additionally, the need for real-time classification precludes the use of full-signal analysis and demands efficient, low-latency models.

2. Materials and method

2.1. Data acquisition system

In essence, the Earth possesses a natural magnetic field composed of extended field lines resembling those of a giant magnet. Magnetic sensors utilize this ambient magnetic field as a baseline reference. Meanwhile, vehicles, comprising metallic components and internal combustion engines, generate their own magnetic fields. As a vehicle passes by a magnetic sensor, it disturbs the surrounding magnetic field. This phenomenon is illustrated in Fig.1.

The data acquisition system prototypes leveraging magnetic field sensors consists of

embedded modules integrated with 3-axis magnetic field sensors. These systems are capable of solar powered operation and are designed to withstand hazard environment conditions. Devices are deployed in a master-slave configuration, where a master unit wirelessly coordinates several slaves. Sensor data collected by the master unit is then transmitted to a PC server through wireless communication for processing and storage. The entire system is powered by proprietary algorithms and software, which are developed and managed on a PC server. As shown in Fig. 2, the system is highly optimized for wide-area management, boasts exceptional integration capabilities, and can be easily replicated on a large scale.

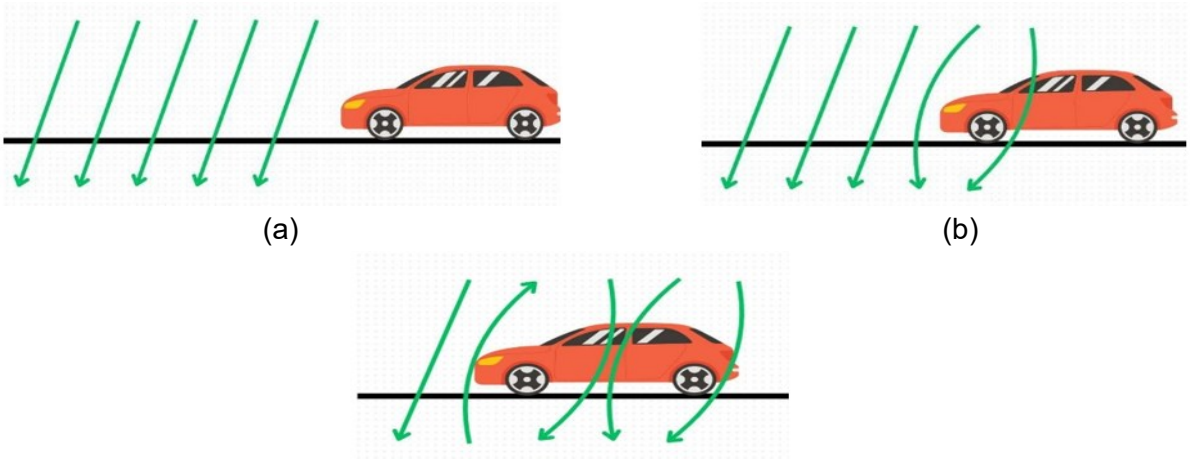

(a) (b)

(c)

Fig. 1. Distortion of local magnetic field at the point of view where the sensor is installed in different situations: vehicle approaching, vehicle nearby and vehicle passing overhead sensor

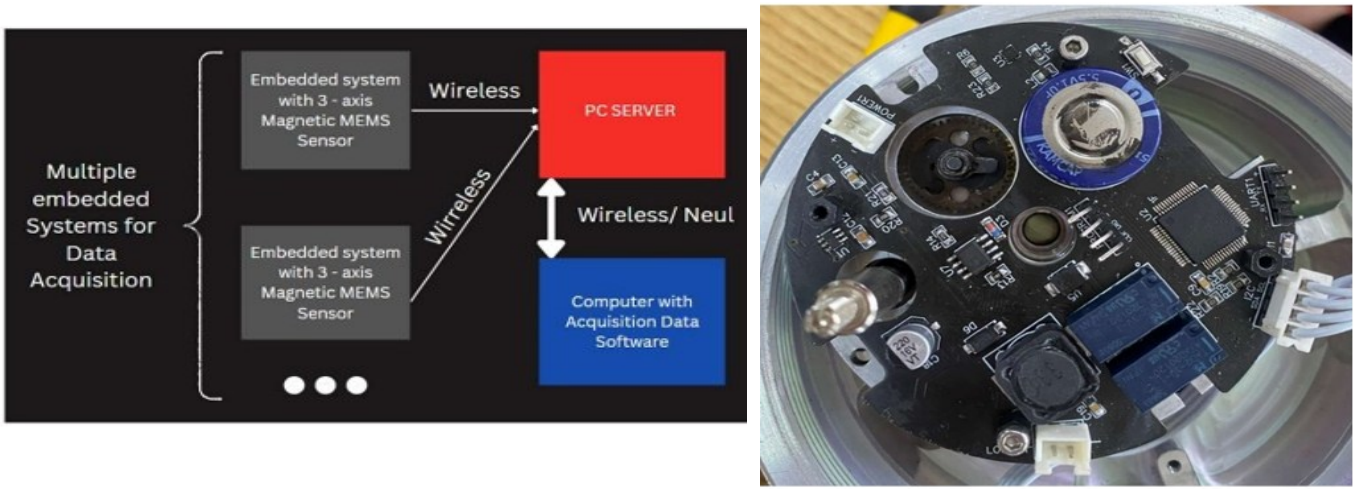

Fig. 2. Operating principal diagram of data acquisition system (left) and Embedded board with a built-in magnetic field sensor LIS3MDL (right) [15]

The experimental setup is illustrated in Fig. 3. Two embedded magnetic field sensor modules were installed approximately one meter apart on the median strip. The Z-axis of the sensors was oriented vertically, perpendicular to the road surface, to enhance sensitivity to vehicles moving overhead. The installation point was located 20 cm from the centerline of the nearest lane, to differentiate between vehicles crossing and passing legally.

Drivers were instructed to operate three types of vehicles—sedans, small trucks, and semi-trucks—across various scenarios. For LEG maneuvers, vehicles were driven in the correct lane, parallel to the median strip. Speeds included slow (~10 km/h), moderate (<60 km/h), and

simulated high-speed (>60 km/h up to 90 km/h) conditions. Since it was not feasible to conduct real experiments at high speeds, data for >60 km/h cases were reconstructed by compressing valid moderate-speed signal windows in time and adding Gaussian noise estimated from the LIS3MDL's typical noise profile. This approach helped emulate real-time disturbances consistent with faster vehicle movement. For ILL maneuvers, the driver deliberately crossed into the lane where the sensor was placed, simulating a lane violation. These trials were repeated multiple times for each vehicle type to ensure data consistency. The sampling rate of the magnetic field data was set at 80 Hz, which was sufficient to capture transient field changes associated with vehicle movement.

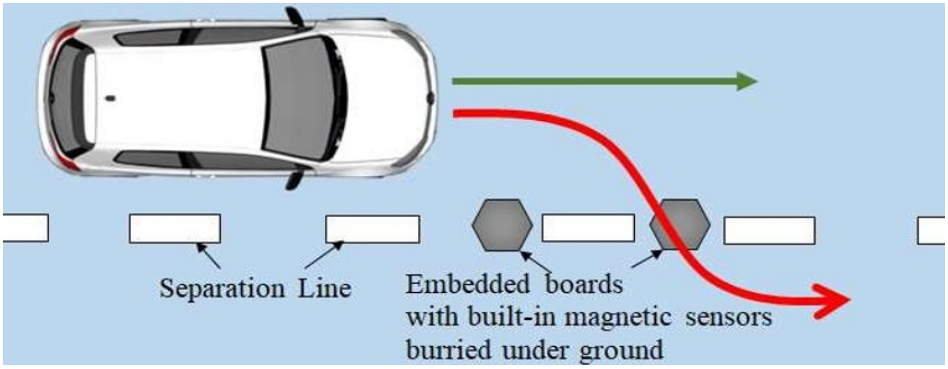

Fig. 3. Experimental setup for data acquisition

2.2. Vehicle behavior classification: feature extraction and classification method

Due to the fact the Earth's magnetic field varies by location, the initial step in signal processing involves extracting changes in the magnetic field vector as measured by the 3-axis magnetic field sensor.

$$\Delta\overline{B} = (\Delta x, \Delta y, \Delta z) \quad (1)$$

$$\Delta x=x-x_0;\ \Delta y=y-y_0;\ \Delta z=z-z_0 \quad (2)$$

Where, x_0, y_0,z_0 - are background magnetic field components in ambient conditions (no vehicle present); and x, y, z are the instantaneous measured values. As it has been considered in many other studies, the presence of a vehicle might be detected via a threshold method, with the magnetic field change threshold typically ranging from 40 and 60 mG [16, 17].

It is evident that the magnetic field changes more significantly when a vehicle passes directly over the sensor than when it passes by the sensor. However, the amplitude of change also varies with different vehicles. Furthermore, the vertical magnetic field component (Z-axis) tends to increase sharply when a vehicle goes overhead the sensor, indicating that the total magnetic field vector aligns more strongly with the vertical direction. Thus, this study focuses on the vertical declination angle α of the magnetic field, defined as:

$$\alpha=\sqrt{\frac{\Delta^2 z}{\Delta^2 x+\Delta^2 y+\Delta^2 z}} \quad (3)$$

To support early-stage detection (e.g., for alerting other subsystems like cameras), only the initial rising portion of the Z-signal is considered. To reinforce this, a new modified Z-component is defined as:

$$Z=|\alpha\times z\,| \quad (4)$$

Fig. 4a illustrates magnetic field variations as a vehicle passes either overhead or beside the sensor. In this example, the patterns of *X*- and *Y*-components differ between the two cases. However, because the sensor orientation in the horizontal plane may vary in practice, *X*- and *Y*-components are not reliable across deployments. In contrast, the *Z*-axis—perpendicular to the road—remains consistent and orientation-invariant, which justifies its selection for feature extraction. Fig. 4b demonstrates the peak detection strategy used to extract the feature

vector from the modified *Z*-component. Specifically, peak detection relies on statistical z-score analysis to identify the first significant change in signal.

Therefore, the Z-component is primarily used for classification. However, it is important to note that the actual input for the neural network is the modified Z-component, which also includes the declination of the magnetic field vector relative to the vertical direction, as described by Equation (3). To ensure rapid detection, only the initial rising portion of the modified *Z*-component is used. A peak detection algorithm based on z-score analysis is applied to locate the first significant deviation [18]. Specifically, at each time index k, the mean and standard deviation of the signal over a historical window of length s are calculated as follows:

$$\mu_Z[k]=\frac{1}{s}\times\sum_{i=0}^{s-1}Z[k-i] \quad (5)$$

$$\sigma_Z[k]=\sqrt{\frac{1}{s-1}\times\sum_{i=0}^{s-1}\left(Z[k-i]-\mu_Z[k]\right)^2} \quad (6)$$

A local peak is then identified at time k+1 if

$$\left|Z[k+1]-\mu_Z[k]\right|>z\_score\times\sigma_Z[k] \quad (7)$$

In practice the constant parameter z-score, is set empirically, typically greater than 3, to ensure only statistically significant peaks are selected. Once the first peak is detected, a feature vector is constructed using the most recent values of the vertical declination angle α: (α[k], α [k-1],…, α[k-M+1]), where the vector length *M* is predefined (Fig. 4b).

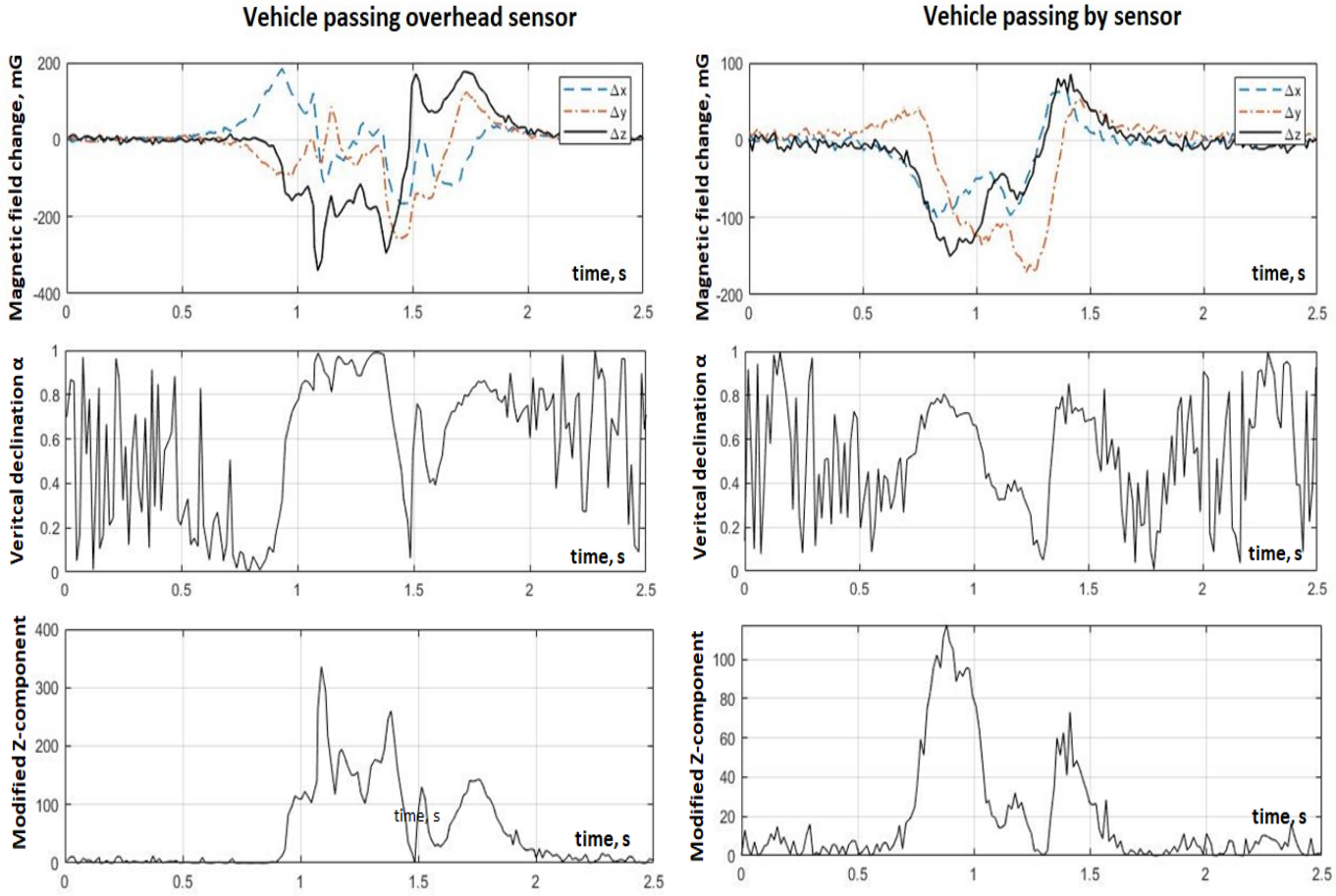

(a)

Fig. 4. a) Illustration of magnetic field variations across the three axes when a vehicle passes directly over the sensor versus when it passes beside the sensor; b) Detection of the first significant peak in the modified Z-component using z-score analysis, followed by feature vector construction based on the vertical declination angle α

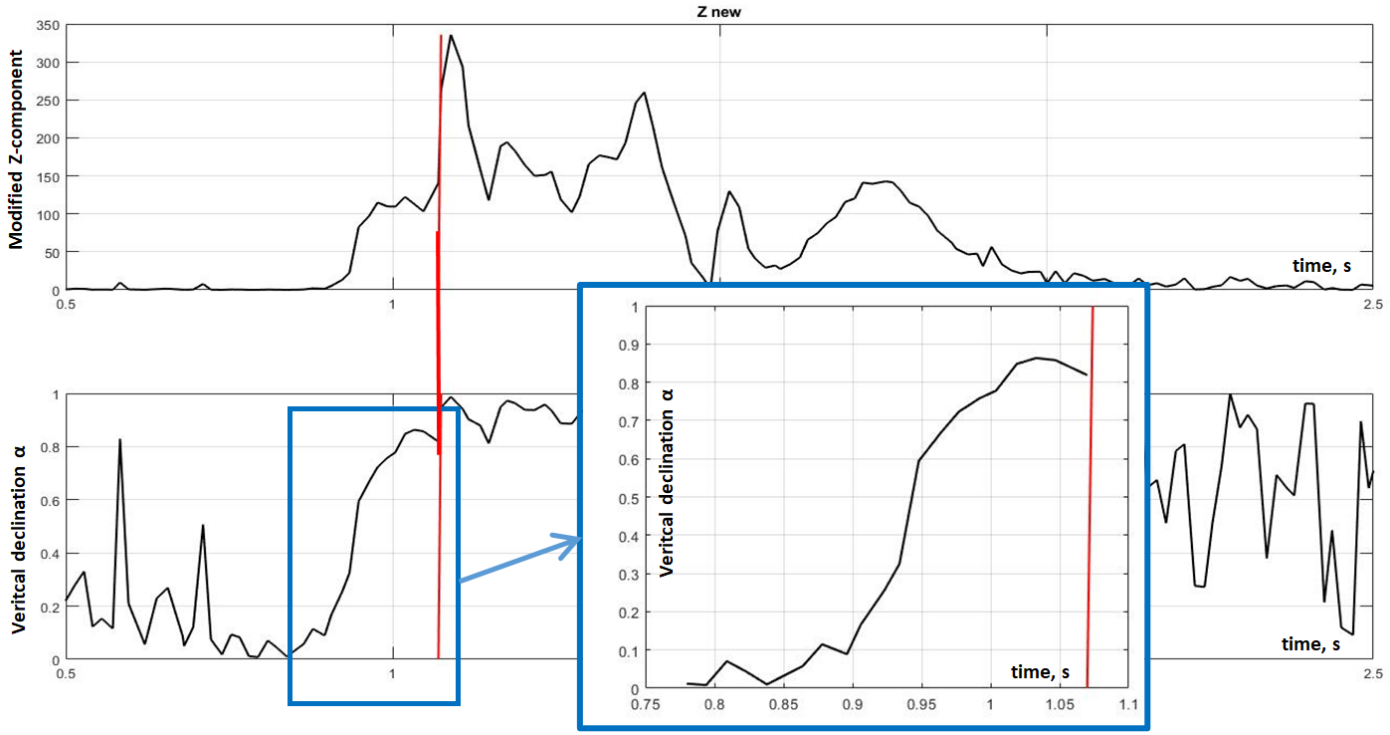

(b)

Fig. 4. (continued)

For classification purposes, a lightweight neural network with a single hidden layer has been designed and trained. The hidden layer consists of 6 neurons, chosen to balance classification performance with low computational cost on embedded hardware. Choosing a hidden layer of 6 neurons based on the Hecht-Nielsen method, the recommended number of hidden neurons in a single-layer neural network should satisfy the following condition [19]:

$$\text{Hidden Neurons} \leq \frac{\text{Training Samples}}{10 \cdot (\text{6-binary classifi})} \quad (8)$$

A total of 976 labeled samples were collected; 75% of these (732 samples) were used for training, and the remaining 25% (244 samples) are used for validation. The data is split into 75% for training and 25% for testing based on the machine learning benchmark for small and medium sized datasets. This ratio strikes a balance between the model's learning ability and the reliability of the real-world evaluation. Choosing the training set as 75% of the dataset ensures that the model is exposed to enough data variability to learn the parameters and generalize the model effectively.

The overall algorithm applied to the embedded device is summarized in Table 1.

Fig. 5 represents the loss of the model, illustrating the relationship between the learning rate and the loss value during the training process. The learning rate, which was selected for computation at 0.0044, falls within the optimal range of 10^{-3} to 10^{-2}, indicating effective model learning and convergence. This choice ensures stability and minimizes the loss, avoiding the instability observed at higher learning rates (above 10^{-1}) or the fluctuations seen between 10^{-2} and 10^{-1}.

Network deployed in the embedded system and the learning curve of the neural network (loss vs iteration).

To justify the choice of the lightweight neural network architecture (single hidden layer with 6 neurons), an additional experiment compared its performance with a deeper model consisting of two hidden layers, each with 12 neurons. The deeper model achieved a marginal accuracy improvement of about 1.5% (96.6% on the validation dataset

(244 samples). However, it increased the latency by ~30% (from <20 ms to ~26 ms) and required higher memory, which is not compatible with embedded hardware. Given the real-time requirements of intelligent transportation systems (ITS) and the need for low-power deployment, the single-layer model was chosen because of its balance between accuracy, low latency, and resource efficiency, designed for embedded systems [20].

Table 1. Algorithm

Objective	Classify vehicle behaviors based on magnetic field sensor signals as either LEG or ILL
Input	Time series data of *X*-, *Y*-, and *Z*- components from the magnetic field sensor
Output	Classification of vehicle behavior: LEGor ILL
Constant Parameters	1. AMPL_THR: Amplitude threshold for signal detection. 2. s: Window length for calculating the initial mean and standard deviation. 3. z-score: Parameter for identifying significant signal deviations (local peaks). 4. M: feature vector length.
STEPS **1. Initialization:** **2. Main Loop (For each time step (k > N):** **3. Repeat:**	- From the first *s* measurements *Z*[1], *Z*[2], ..., *Z*[*s*], calculate: - Initial mean: μ_Z - Initial standard deviation: σ_Z a. Compute the current values: - Calculate the current magnitude *Z*[*k*] (the signal's strength at time *k*). - Calculate α[k] based on the signal processing step. b. Detect significant peaks: - Check if the following conditions are met: 1. *Z*[k] > AMPL_THR (the signal exceeds the amplitude threshold). 2. |*Z*[k] - μ_Z| > z_score × σ_Z) (the signal deviates significantly from the mean). c. Create the feature vector: - If both conditions are true, form the feature vector (*Z*[*k*], *Z*[*k*-1], ..., *Z*[*k*-M+1]) d. Classify behavior: - Use the feature vector as input to a Neural Network to classify the vehicle's behavior as LEG orILL. e. Update statistical quantities: - Update the mean μ_Z and standard deviation σ_Z with the new data *Z*[*k*]. - The process continues for each new time step *k*.

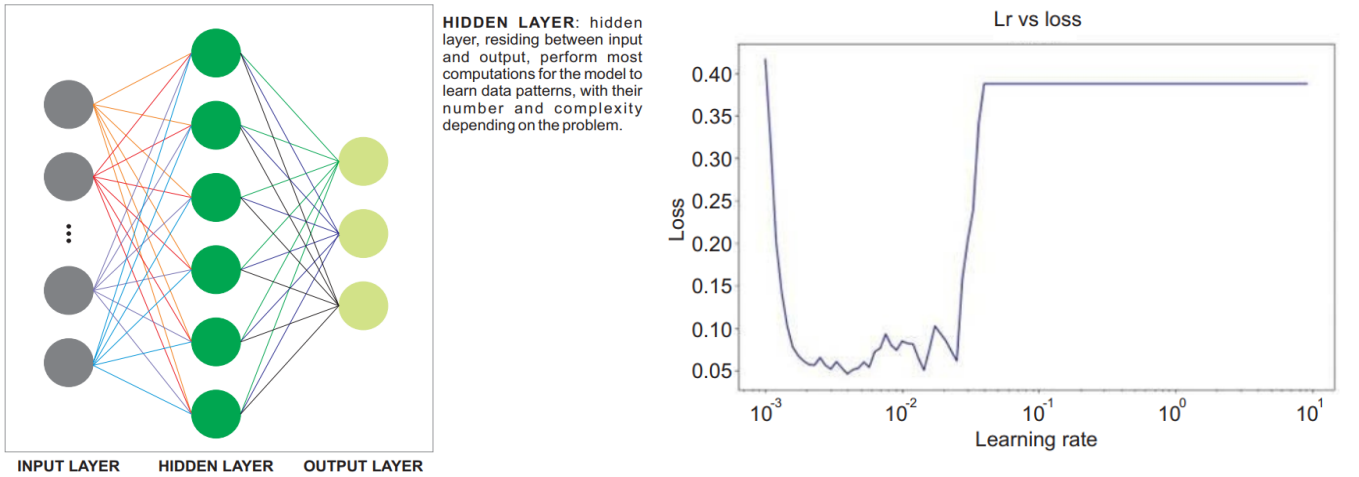

Fig. 5. Architecture of the light weighted neural

2.3. Validation metrics

The performance of the classification model is evaluated using standard metrics derived from the confusion matrix. The confusion matrix summarizes the classification results by displaying the counts of correctly and incorrectly predicted

instances for each class. It includes four fundamental components [21]:

- True Positive (TP): The number of ILL behaviors correctly predicted as ILL.

- True Negative (TN): The number of LEG behaviors correctly predicted as LEG.

- False Positive (FP): The number of LEG behaviors incorrectly predicted as ILL.

- False Negative (FN): The number of ILL behaviors incorrectly predicted as LEG.

These components are obtained from the neural network's classification output by applying a default threshold classifier to separate the two classes [22]. The confusion matrix provides a clear overview of how effectively the model distinguishes between classes.

Additionally, the metrics of Accuracy, Precision, Recall, and F1-Score are used for quantitative performance evaluation. Accuracy represents the overall proportion of correct predictions (TP + TN) relative to the total number of samples. Precision and Recall specifically target the ILL class to assess the model's capability in detecting traffic violations:

- Precision measures the proportion of correctly predicted ILL instances among all instances predicted as ILL.

- Recall (or sensitivity) measures the proportion of correctly identified ILL behaviors relative to all actual ILL behaviors.

The F1-Score combines Precision and Recall into a single metric, providing a balanced evaluation of the model's effectiveness in recognizing violations. To ensure reliable deployment on embedded devices, these evaluation metrics were calculated using an optimized and lightweight neural network model [19]. The evaluation was performed with randomly split datasets to verify stability and reproducibility [21].

Furthermore, the Area Under the ROC Curve (AUC) was employed to quantify the model's discriminatory capability between the LEG and ILL classes. The AUC value ranges from 0 to 1, where values closer to 1 indicate superior classification performance. In our evaluation process, the AUC metric was obtained through multiple validation runs, ensuring robustness and reliability. Additionally, the test dataset underwent noise reduction preprocessing, consistent with approaches applied in prior vehicle classification studies using magnetic field signals [23].

3. Results and discussion

3.1. Optimizing parameters of the model

To ensure high performance vehicle behavior classification system, the parameters AMPL_THR, s, z-score, and M were optimized using a grid search method, following hyperparameter tuning [21]. These parameters are important to the system's signal processing and classification: AMPL_THR defines the amplitude threshold for detecting magnetic field changes, s decides the window length for computing statistical measures, z-score fixes the threshold for peak detection, and M specifies the length of the feature vector based on the vertical declination angle. A grid search was conducted to explore combinations of parameter values, evaluating performance on the validation dataset (25% of the 976 samples, or 244 samples). The parameter ranges tested are listed: AMPL_THR from 40 to 80 mG (step size: 10 mG), s from 3 to 10 samples (step size: 1), z-score from 2.5 to 4.5 (step size: 0.5), and M from 6 to 12 (step size: 2). The selection standard was maximizing classification accuracy on the validation set while ensuring processing latency remained below 20 ms on embedded hardware. The optimal numbers are selected based on the high mean accuracy while maintaining latency constraints, summarized in Table 2.

Table 2. Hyperparameter optimization results

Parameter	Range	Optimal Value
AMPL_THR	40–80 mG	40 mG
s	3–10 samples	5
z-score	2.5–4.5	3.5
M	6–12	6

The optimal AMPL_THR is 40 mG which ensures detection of magnetic interference while

minimizing false positives from environmental noise. 5 samples balance statistical stability and low latency, which is important for real-time embedded system. The z-score threshold of 3.5, supported by peak detection literature [22], effectively identifies significant signal deviations. A feature vector length of 6 provides sufficient information without increasing computational complexity. This configuration achieves a validation accuracy of 96.6% and maintains a processing latency of less than 20 ms, making it suitable for deployment on low-power embedded platforms.

3.2. Validation of the model

The dataset used for evaluation was constructed based on experimental measurements, as described in Section 2. Due to limitations in the physical testing environment, vehicle speeds during the experiment were restricted to below 50 km/h. To simulate higher-speed scenarios (up to 90 km/h), signal windows from valid low-speed data were compressed in the time domain and augmented with white Gaussian noise. This synthetic augmentation was carried out carefully to preserve the statistical properties of actual high-speed signals, ensuring realistic evaluation. The dataset includes three vehicle types (e.g., sedan, small truck, semi-truck), each tested under approximately 50 different scenarios. The sensor sampling period was set to approximately 12 milliseconds, corresponding to a sampling rate of 80 Hz. The embedded classification algorithm was optimized not only for accuracy but also for low power consumption. From the moment a magnetic disturbance begins, the system generates a classification decision within 20 milliseconds, as measured by oscilloscope trigger timing between input detection and output response.

In Fig.6, after the first 20 epochs the model has achieved stability indicating efficient learning and the consistently high accuracy/loss values indicate robustness and reliability. Loss (orange) decreases sharply and stabilizes near 0, Accuracy starts low and increases rapidly, Val Accuracy quickly reaches and maintains a high value (close to 1), Val Loss (red) drops to near 0 and remains low. This shows that the model does not overfit, ensuring the model performs well.

The analysis of the provided data reveals that the model exhibits exceptional performance across both training and testing phases, with its reliability and effectiveness for the given classification task. During training, the model achieves strong convergence, as evidenced by high accuracy (95%) and validation accuracy values paired with low loss and validation loss (92%), indicating effective learning of underlying patterns without significant overfitting (Table 3).

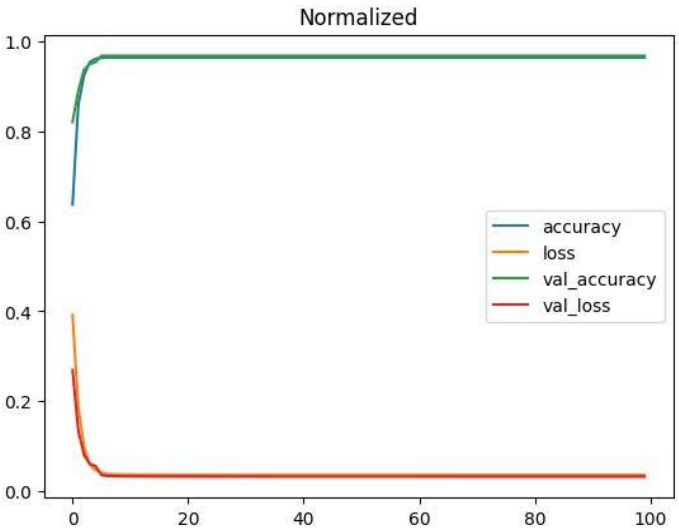

Fig. 6. Training and validation metrics

Table 3. Model training performance metrics

Metric	Value
Training Accuracy	95%
Training Loss	0.05
Validation Accuracy	92%
Validation Loss	0.08

The classification results are also summarized in Table 4, which is presented based on Confusion Matrix. Fig. 7 shows the performance of a classification model for LEG and ILL classes, with true positives, true negatives, false positives, and false negatives. True LEG: 307 (98.4%), False ILL: 11 (6.2%), False LEG: 5 (1.6%), and True ILL: 166 (93.8%). The model is highly effective with low error rates (1.6% and 6.2%), high accuracy (98.4%

for LEG, 93.8% for ILL), and minimal misclassifications, indicating strong performance and reliability.

Table 4. Confusion matrix for testing the model

Output behavior	LEG	98.4%	1.6%
	ILL	6.2%	93.8 %
		LEG	ILL
		Target behavior	

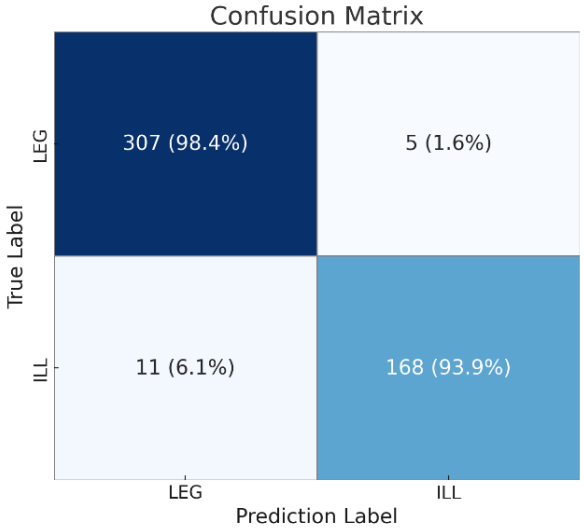

Fig. 7. Confusion matrix of for training the model

Fig. 8 illustrating the model's performance based on ROC analysis based on the testing data. The results show that the area under the ROC curve class LEG is 0.96 (AUC = 0.96) while this value for class ILL is 0.96 (AUC = 0.96), both showing high performance, alongside the micro-average ROC (AUC = 0.97) and macro-average ROC (AUC = 0.97), reflecting the overall and unweighted average model performance respectively, with all AUC values ranging from 0.96 to 0.97.

Table 5. Model performance metrics using testing dataset

Metric	LEG	ILL	Overall
Precision	99%	98%	98.5%
Recall	98.4%	93.8%	96.1%
F1 Score	97.4%	95.4%	96.4%
Testing Accuracy			96.6%
AUC			97%

We have also calculated other metrics during the testing phrase. Table 5 shows the Recall scores are 0.984 for the LEG class and 0.938 for the ILL class, indicating strong ability to correctly identify actual samples. The F1 Scores, balancing precision and recall, are 0.97 for LEG and 0.95 for ILL, demonstrating high effectiveness across both classes. Overall model performance is reflected by an accuracy of 96.6% and AUC values from the ROC curve ranging from 0.96 to 0.97 (Micro/Macro), confirming excellent discriminative power and stability during training.

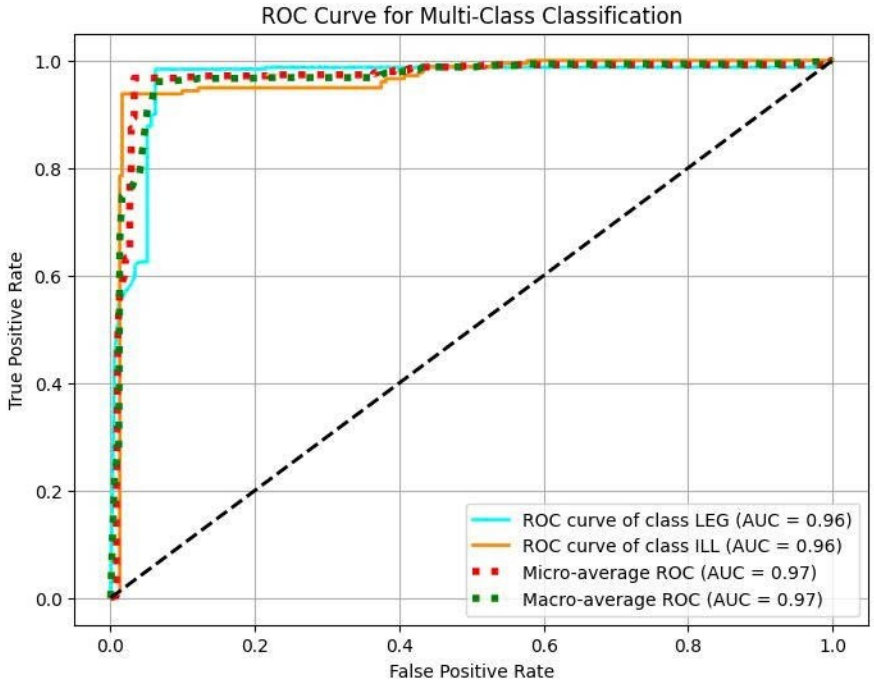

Fig. 8. ROC Curve of the model trained

The results also show that the model performance remains robust, boasting an overall accuracy of 96.6%, an F1 score of 96%, and an AUC of 0.97, highlighting its impressive generalization capabilities. The confusion matrix confirms this by showing a high number of correct predictions with minimal misclassifications between the two classes, while the ROC curves for both classes (LEG and ILL) yield AUC values of 0.96, with micro-average and macro-average AUCs reaching 0.97. The model is impressive in detecting illegal maneuvers, characterized by distinct, high-amplitude changes in the Z-component of the magnetic field. However, it exhibits a slightly higher false-positive rate for legal behaviors, primarily due to heavy vehicles like trucks passing close to the sensor without crossing the lane, generating strong magnetic signatures akin to illegal acts because of their size and metallic mass. This limitation, noted for future improvement, could potentially be mitigated through sensor fusion or contextual constraints such as speed or vehicle classification. Despite this, the model's compact architecture, fast runtime, and overall accuracy of 96.6% affirm its suitability for real-time embedded deployment, with its low-latency and energy-efficient design making it an ideal solution for infrastructure-constrained or weather-affected environments where traditional camera or loop-based systems may falter.

3.3. Limitations of simulated high-speed data

The simulation technique is shown to be consistent with establish literature in sensor signal processing [21, 22]. Signal compression preserves the temporal structure of the magnetic noise, while the addition of Gaussian noise simulates the typical noise profile of the sensor, ensuring statistical consistency with the real signal [21]. Real-world high-speed testing is not able due to limited access to controlled highway environments and safety concerns, making simulation a practical alternative for proof-of-concept evaluation [21].

To address these limitations, future work will prioritize collecting a small dataset of realistic high-speed data (e.g., 10–20 samples) in a controlled highway setting to validate the performance of the model. Additionally, advanced simulation techniques, such as physics-based models of vehicle magnetic fields, could enhance the reliability of the data. These improvements would increase the applicability of the system to a variety of traffic conditions. Despite the limitations, the system's 96.6% authentication accuracy on calibrated high-speed data demonstrates its feasibility for urban environments where speeds typically remain below 60 km/h. Ongoing research will focus on closing this gap to ensure robust performance under all conditions.

3.4. Comparing with existing system

In this section, three announced methods are compared with our method, those there are: vision-based systems using cameras and artificial intelligence (AI) [23], and multi-sensor magnetic arrays [24], inductive loop systems [25], summarized in Table 6.

Table 6. Comparison of this study with published works

System	Accuracy	Latency (ms)	Against environmental impact
Proposed (Single Magnetic Sensor + NN)	96.6%	20	High
Inductive loop systems [23]	85%	30-50	Moderate
Multi-sensor magnetic arrays [22]	90%	25-40	High
Vision-based [21]	95%	50-100	Low

Vision-based system using camera and deep learning algorithms, allows it to have high accuracy up to 96% under optimal conditions [26]. However, the system requires high-performance hardware, weak when again harsh conditions. Multi-sensor magnetic arrays achieve 90% accuracy [27]. But

deploying in a wide area cost high. Inductive loop systems only reach 85% accuracy and high latency make it become a not recommended system.

4. Conclusion

In this paper, we have presented an approach to solving a very practical problem a practical and lightweight approach for detecting vehicle behavior specifically, determining whether a vehicle crosses the lane line illegally using a single 3-axis magnetic field sensor. The proposed method utilizes a z-score-based algorithm to extract real-time features related to vertical magnetic field declination and employs a compact neural network model to classify legal versus illegal lane behavior. The classification model has achieved an overall accuracy rate of 96.6%, demonstrating the feasibility of deploying this system on low-power embedded hardware in real-world traffic scenarios. Future work may focus on expanding the range of vehicle types and traffic conditions evaluated, as well as incorporating multi-sensor fusion on temporal modelling to further improve classification robustness. In addition to expanding the dataset and incorporating multiple sensor fusion, future research could aim to extract orientation-invariant features from the X and Y components of the magnetic field to enhance the robustness of the classification. The current system relies primarily on the Z component due to its consistency across implementations, but the X and Y components could contain additional useful information with sensor orientation variations. Techniques such as spectral analysis or orientation-invariant transforms, as demonstrated in prior work, could provide more good features from these components, improving performance in scenarios with variable sensor orientations. This direction promises to improve the system's adaptability for diverse real-world applications.

Acknowledgement

This research was financially supported by Hanoi University of Science and Technology with Project number T2024-TĐ-028.

References

[1]. C. Premebida, G. Monteiro, U. Nunes, P. Peixoto. (2007). A lidar and vision-based approach for pedestrian and vehicle detection and tracking. *2007 IEEE Intelligent Transportation Systems Conference, pp.1044-1049.* https://doi.org/10.1109/ITSC.2007.4357637

[2]. S.S. Islam, K. Dey, M.R. Islam, M.K. Alam. (2012). An infrared based intelligent Traffic System. *2012 International Conference on Informatics, Electronics & Vision (ICIEV)*, pp. 57-60. http://dx.doi.org/10.1109/ICIEV.2012.6317334

[3]. V.-S. Ha, N.T.B. Hien. (2024). Machine Learning Models for Real-Time Traffic Prediction: A Case Study in Urban Traffic Management. *Journal of Science and Transport Technology*, 4(2), 1-12. https://doi.org/10.58845/jstt.utt.2024.en.4.2.1-12

[4]. E. Odat, J.S. Shamma, C. Claudel. (2017). Vehicle classification and speed estimation using combined passive infrared/ultrasonic sensors. *IEEE Transactions on Intelligent Transportation Systems,* 19, (5), 1593-1606. https://doi.org/10.1109/TITS.2017.2727224

[5]. K. Shaaban, M. Elamin, M. Alsoub. (2021). Intelligent transportation systems in a developing country: benefits and challenges of implementation. *Transportation Research Procedia*, 55, 1373-1380. https://doi.org/10.1016/j.trpro.2021.07.122

[6]. S.Y. Cheung, S. Coleri, B. Dundar, S. Ganesh, C-W. Tan, P. Varaiya. (2005). Traffic measurement and vehicle classification with single magnetic sensor. *Transportation Research Record: Journal of the Transportation Research Board*, 1917(1), 173-181. https://doi.org/10.1177/0361198105191700119

[7]. Y. Feng, G. Mao, B. Chen, C. Li, Y. Hui, Z. Xu, J. Chen. (2022). MagMonitor: Vehicle speed estimation and vehicle classification through a magnetic sensor. *IEEE Transactions on*

Intelligent Transportation Systems, 23(2), 1311-1322. https://doi.org/10.1109/TITS.2020.3024652

[8]. Q. Wei, B. Yang. (2017). Adaptable vehicle detection and speed estimation for changeable urban traffic with anisotropic magnetoresistive sensors. *IEEE Sensors Journal*, 17(7), 2021-2028. https://doi.org/10.1109/JSEN.2017.2654501

[9]. P. Gorzelanczyk. (2023). Using neural networks to forecast the number of road accidents in Poland taking into account weather conditions. *Results in Engineering*, 17(1), 100981. http://dx.doi.org/10.1016/j.rineng.2023.100981

[10]. Project on Strengthening the National Road Safety Management Capacities of Selected Developing Countries, and Countries with Economies in Transition, Funded by the United Nations Development Account. (2018). United Nations economic and social commission for Asia and the Pacific, Road safety performance review Viet Nam. Available: https://unece.org/DAM/trans/roadsafe/unda/RSPR_Viet_Nam_FULL_e.pdf

[11]. V.L. Giap, T.A. Pham. (2024). Developing a Machine Learning Model for Predicting the Settlement of Bored Piles. *Journal of Science and Transport Technology*, 4(4), 95-109. https://doi.org/10.58845/jstt.utt.2024.en.4.4.95-109

[12]. M.V. Le, I. Prakash, D.D. Nguyen. (2023). Predicting load-deflection of composite concrete bridges using machine learning models. *Journal of Science and Transport Technology*, 3(4), 43-51. https://doi.org/10.58845/jstt.utt.2023.en.3.4.43-51

[13]. D.V. Tran, T.-H.T. Hoang, H.-B. Ly. (2024). Enhancing Inland Waterway Safety and Management through Machine Learning-Based Ship Detection. *Journal of Science and Transport Technology*, 4(3), 39-52. https://doi.org/10.58845/jstt.utt.2024.en.4.3.39-52

[14]. Q.B. Vo, T.-H.T. Nguyen, T-H.T. Hoang, D.T. Tran, H.-B. Ly. (2025). Enhancing construction safety management efficiency with AI-Powered real-time helmet detection. *Journal of Science and Transport Technology*, 5(1), 77-91. https://doi.org/10.58845/jstt.utt.2025.en.5.1.77-91

[15]. STMicroelectronics NV Company. (2023). Datasheet of magnetic sensor LIS3MDL. Available: https://www.st.com/resource/en/datasheet/lis3mdl.pdf

[16]. A. Haoui, R. Kavaler, P. Varaiya. (2008). Wireless magnetic sensors for traffic surveillance. *Transportation Research Part C: Emerging Technologies*, 16(3), 294-306. https://doi.org/10.1016/j.trc.2007.10.004

[17]. H. Zhu, F. Yu. (2016). A cross-correlation technique for vehicle detections in wireless magnetic sensor network. *IEEE Sensors Journal*, 16(11), 4484-4494. https://doi.org/10.1109/JSEN.2016.2523601

[18]. G.K. Palshikar. (2009). Simple algorithms for peak detection in time-series. In Proc. 1st Int. Conf. advanced data analysis, business analytics and intelligence (Vol. 122).

[19] R.H-Nielsen. (1992). Theory of the backpropagation neural network. *Neural Networks for Perception*, 65-93. https://doi.org/10.1016/B978-0-12-741252-8.50010-8

[20]. S. Han, H. Mao, W. Dally. (2015). Deep compression: Compressing deep neural network with pruning, trained quantization and huffman coding. *International Conference on Learning Representations*. https://doi.org/10.48550/arXiv.1510.00149

[21]. J. Bergstra, Y. Bengio. (2012). Random search for hyper-parameter optimization. *Journal of Machine Learning Research*, 13(1), 281-305.

[22]. B. Yang, Y. Lei. (2014). Vehicle detection and classification for low-speed congested traffic with anisotropic magnetoresistive sensor.

IEEE Sensors Journal, 15(2), 1132-1138. https://doi.org/10.1109/JSEN.2014.2359014

[23]. M.I. Pavel, S. Y. Tan, A. Abdullah. (2022). Vision-based autonomous vehicle systems based on deep learning: A systematic literature review. *Applied Sciences*, 12(14), 6831. https://doi.org/10.3390/app12146831

[24]. B. Coifman, S.B. Kim. (2009). Speed estimation and length based vehicle classification from freeway single-loop detectors. *Transportation Research Part C: Emerging Technologies*, 17(4), 349-364. https://doi.org/10.1016/j.trc.2009.01.004

[25]. S. Saponara, B. Neri. (2017). Radar sensor signal acquisition and multidimensional FFT processing for surveillance applications in transport systems. *IEEE Transactions on Instrumentation and Measurement*, 66(4), 604-615. https://doi.org/10.1109/TIM.2016.2640518

[26]. J. Lan, Y. Xiang, L. Wang, Y. Shi. (2011). Vehicle detection and classification by measuring and processing magnetic signal. *Measurement*, 44(1), 174-180. https://doi.org/10.1016/j.measurement.2010.09.044

[27]. D.M.W. Powers. (2011). Evaluation: from precision, recall and F-measure to ROC, informedness, markedness and correlation. arXiv. https://doi.org/10.48550/arXiv.2010.16061